Eur. Phys. J. Special Topics **226**, 1123–1135 (2017)

DOI: 10.1140/epjst/e2016-60227-3

THE EUROPEAN PHYSICAL JOURNAL SPECIAL TOPICS

Regular Article

Thermodynamic properties of gold-rare earth elements*

Samira Otmani[a], Rkia Tamim, Driss Moustaine, and Kamal Mahdouk

Laboratory of Thermodynamics and Energetics, Faculty of sciences, Ibn Zohr University, BP 8106, 80006 Agadir, Morocco

Received 15 July 2016 / Received in final form 29 September 2016
Published online 18 April 2017

Abstract. This work presents the results of the thermodynamic optimizations of several Au-RE (RE = Ce, Nd, Sm, Eu, Gd, Tb, Dy and Yb) binary phase diagrams using the CALPHAD approach [D. Moustaine, K. Mahdouk, J. Alloys Comp. **683**, 599 (2016); **673**, 115 (2016); S. Otmani, K. Mahdouk, J. Alloys Comp. **670**, 369 (2016); **648**, 581 (2015)]. We compare and discuss, in this study, the alloying behavior as well as the evolution of multiple thermodynamic data relative to the Au-RE phases versus the atomic number of the RE element.

1 Introduction

Because of their greatest properties which make them a fundamental component in a great number of new technologies, the gold-rare earth (RE) intermetallics have been widely studied and the increasing number of publications in this domain over the last few years reflects this interest. We found them used in the bulk of the material or at the contact surface in order to protect them against corrosion in various environments [5]. They have also increasingly been used in Micro-Electro-Mechanical Systems (MEMS) packaging in order to promote bonding [6,8]. Au-RE intermetallics are also used as anti-theft markers for the sensing of physical parameters (pressure, temperature, liquid viscosity and density, fluid flow rate, humidity and gas sensing) [9].

The rare earths and gold generally present low reciprocal solubility; they react with each other giving a great number of intermetallic compounds, characterized by high thermal stability, as can be inferred from the values of their heat of formation and melting points. It is worth noting that Au-Yb and Au-Eu systems are the exception as showed in the following sections.

To utilize the full technological potential of the Au-RE alloys, it is essential to have a fundamental knowledge about them, such as information concerning the phase equilibrium and the related thermodynamic data. In this sense the aims of this work is to compile all the available experimental information, to confirm its consistency and to create an optimized set of data by using the CALPHAD (CALculation of PHAse Diagram) approach [10]. The philosophy of this technique is to obtain a consistent description of the phase diagram and the thermodynamic properties of stable and

* Supplementary material in the form of one pdf file available from the Journal web page at http://dx.doi.org/10.1140/epjst/e2016-60227-3

[a] e-mail: samira.otmani@edu.uiz.ac.ma

metastable phases in regions during simulations of phase transformations applying a mathematical model containing adjustable parameters as well as little experimental data selected from literature.

After having assessed the phase diagrams of the following Au-RE systems: Au-Ce, Au-Nd, Au-Sm, Au-Eu, Au-Gd, Au-Tb, Au-Dy, Au-Yb, by using the CALPHAD approach, we compare in this work the variation of multiple thermodynamic data of those alloys. Assessments and comparison done in this work provide a systematic variation of the Au-RE thermodynamic properties in their dependence on the atomic number of the RE element.

2 Review of the literature data

Gold/rare earth phase diagrams are generally similar except for Au-Yb and Au-Eu systems which contains new phases. Au-RE phases generally crystallizes in 18 crystal structure-type. The equiatomic AuRE phase (1:1) is present in all these systems and his corresponding melting temperature increases with increasing atomic number of the rare earth element. We mention the existence of the $AuRE_2$, Au_2RE, $Au_{51}RE_{14}$, Au_6RE, Au_3RE and Au_4RE phases in the majority of Au-RE phase diagrams as shown in Table 1 which includes all the phases present in these systems as well as their type of transformation with corresponding temperatures.

Various experimental works on Au-RE systems were done by several authors among which the extensive study conducted by McMasters et al. [23] to establish the crystallographic structures of the Au-RE intermetallic compounds and the work by Rider et al. [24] to determine the Au-RE solid solutions boundaries. The Au-RE standard enthalpies of formation available in the literature are the result of experimental measurements [25–33] and "ab Initio" calculations. Figures 6–9 include all the standard enthalpies determined previously by several authors with those calculated for the first time in this work because not yet available in the literature.

3 Thermodynamic assessment

The thermodynamic parameters of each Au-RE phase were optimized by means the CALPHAD method using the PARROT [25] module of Thermo-Calc [26] software. The philosophy of this technique is to obtain a consistent description of the Au-RE phase diagrams and their relative thermodynamic properties. Hence we collect and assess all available experimental and theoretical information available on phase equilibria and thermochemical properties of the studied system. The Gibbs free energy of each studied phase is then described through a mathematical model containing adjustable parameters. These parameters are evaluated by optimizing the fit of the selected model to all the assessed information relative to the studied phase. Following this it is possible to calculate the phase diagram, as well as the thermodynamic properties of all the phases. The obtained parameters can be used as starting information to build multicomponent phase diagrams containing Au and RE elements.

The modeling procedure includes several steps. First, the creation of the TDB file in which the Gibbs energy function of pure elements are recuperated from the Thermo-Calc database [28] while the Gibbs energies of the studied phases are mathematically expressed by means of a Redlich-Kister formalism [27] and the Kaptay model [50] generating parameters to be optimized. The selected experimental thermodynamic quantities and phase diagram information are expressed in POP files. Then the thermodynamic parameters were evaluated using a recurrent runs of the PARROT module of the Thermo-Calc software [26]. As a first step, we introduce a file in which we express the stability of the liquid phase in order to avoid its demixing

Table 1. Type of reactions and their corresponding temperatures (in Kelvin) of Au-RE intermetallic compounds. (P: Peritectic transformation, C: Congruent melting).

RE:Au / RE	0.25	0.3	0.33	0.375	0.4	0.44	0.5	0.55	0.538	0.571	0.588	0.66	0.679	0.75	0.784	0.8	0.833	0.857
	3:1	7:3	2:1	5:3	3:2	5:4	1:1	9:11	6:7	3:4	7:10	1:2	17:36	1:3	14:51	1:4	1:5	1:6
La [11]	–	–	P 941	–	–	–	C 1596	–	–	–	–	C 1490	–	–	C 1477	–	–	P 1175
Ce [12]	–	–	P 992	–	–	–	C 1643	P 1470	–	–	–	C 1479	–	–	C 1493	–	–	P 1077
Pr [13]	–	–	P 1023	–	–	–	C 1693	–	–		–	P 1363	–	–	C 1483	–	–	P 1073
Nd [14]	–	–	P 1083	–	–	–	C 1743	–	–	P 1353	–	–	C 1443	–	C 1483	–	–	P 1148
Pm [15]	–	–	P 1122	–	–	–	C 1732	–	–	–	–	C 1469	–	–	C 1469	–	–	
Sm [16]	–	–	P 1138	–	–	–	C 1798	–	P 1443	–		C 1453	–	P 1135	C 1483	–	–	P 1073
Eu [17]	P 773	P 838	–	–	P 1028	–	C 1293	–	–	–	–	C 1358	–	–	–	P 1178	C 1248	–
Gd [18]	–	–	P 1208	–	–	–	C 1858	–	–	P 1613	P 1433	C 1453	–	C 1473	C 1438	–	–	P 1128
Tb [19]	–	–	P 1273	–	–	–	C 1863	–	–	P 1613	P 1483	C 1538	–	C 1488	P 1448	–	–	P 1128
Dy [16]	–	–	P	–	–	–	C 1933	–	–	–	–	c	–	c	P	–	–	p
Ho [20]	–	–	P 1368	–	–	–	C 1973	–	–	–	P 1622	C 1609	–	C 1519	P 1333	P 1224	–	P 1115
Er [20]	–	–	P 1387	–	–	–	C 1979	–	–	–	P 1635	C 1638	–	C 1553	–	P 1274	–	–
Tm [20]	–	–	P 1433	–	–	–	C 1993	–	–	–	P 1618	C 1703	–	C 1573	–	P 1308	–	–
Yb [21]	–	P 934	P 985	P 1134	–	P 1199	C 1565	–	–	–	–	C 1513	–	C 1423	–	P 1262	–	–
Lu [22]	–	–	P 1604	–	–	–	C 2053	–	–	–	–	C 1403	–	–		P 1248	–	–

especially at high temperatures. For this reason, a positive curvature of the liquidus was added by imposing the additional constraint in the whole atomic composition range up to 4600 K [29,30]. In a next step we introduce the congruent equilibrium occurring in those systems. Then we treat each invariant equilibrium separately until a better fit of the experimental phase diagram is reached. Particular attention was given to the evaluation of the optimized parameters at each step of the calculation process and each piece of experimental information is given a certain weight according to its estimated accuracy. The weights were changed systematically during the assessment until most of the selected experimental data were accounted for within the claimed uncertainty limits.

The liquid and the solid solution phases were considered as substitutional solutions. Their thermodynamic excess Gibbs energy was fitted by Redlich-Kister [27] polynomials. The intermetallic compounds were treated as stoichiometric phases since no experimental information relative to their homogeneity range is known.

3.1 Pure elements

The Gibbs energy function: ${}^{0}G_i^{\varphi}(T) = G_i^{\varphi} - H_i^{SER}\ (298.15\,\mathrm{K})$ for the element "i" in the phase φ (φ = Liquid, hcp_A3, fcc_A1 and bcc_A2) is described by an equation of the following form:

$$ {}^{0}G_i^{\varphi}(T) = a + bT + cT\ln T + dT^2 + eT^3 + fT^7 + gT^{-1} + hT^{-9} \tag{1} $$

where is H_i^{SER} (298.5 K) the molar enthalpy of the element "i" at 298.15 K in its standard element reference (SER) state: hcp_ A3 or bcc_ A2 for the RE element and fcc_ A1 for Au.

In this work, the Gibbs energy functions are taken from the Scientific Group Thermodata Europe (SGTE) compilation of Dinsdale [28].

3.2 Solution phases

The liquid, (αRE/βRE) and (Au) solution phases are modeled as substitutional solutions according to the Redlich-Kister polynomial formalism [27]. The Gibbs energy "G_m^{φ}" of one mol of formula unit of the φ phase is expressed as the sum of the reference part ${}^{ref}G^{\varphi}$ the ideal part ${}^{id}G^{\varphi}$ and the excess part ${}^{xs}G^{\varphi}$:

$$ G_m^{\varphi} = {}^{ref}G^{\varphi} + {}^{id}G^{\varphi} + {}^{xs}G^{\varphi} \tag{2} $$

where:

$$ \begin{aligned} {}^{ref}G^{\varphi}(T) = &\left({}^{\circ}G_{RE}^{\varphi}(T) - H_{RE}^{SER}(298.15\,K)\right)x_{RE} \\ &+ \left({}^{\circ}G_{Au}^{\varphi}(T) - H_{Au}^{SER}(298.15K)\right)x_{Au} \end{aligned} \tag{3} $$

$$ {}^{id}G^{\varphi} = RT\left(x_{RE}\ln x_{RE} + x_{Au}\ln x_{Au}\right). \tag{4} $$

The excess terms were modeled by the Redlich-Kister [27] polynomial formalism:

$$ \begin{aligned} {}^{xs}G_m^{\varphi}(T) = x_{RE}x_{Au}[&{}^{\circ}L_{RE,Au}^{\varphi}(T) + {}^{1}L_{RE,Au}^{\varphi}(T)(x_{RE} - x_{Au}) \\ &+ {}^{2}L_{RE,Au}^{\varphi}(T)(x_{RE} - x_{Au})^2 + ...] \end{aligned} \tag{5} $$

where, ${}^{i}L_{RE,Au}^{\varphi}(T) = a_i + b_iT$ is the interaction parameter between the elements RE and Au, which is evaluated in this study by optimizing the a_i and b_i terms using the PARROT module [25]. T is the temperature in Kelvin, R is the gas constant, while x_{RE} and x_{Au} are the mole fraction of the RE and Au elements respectively.

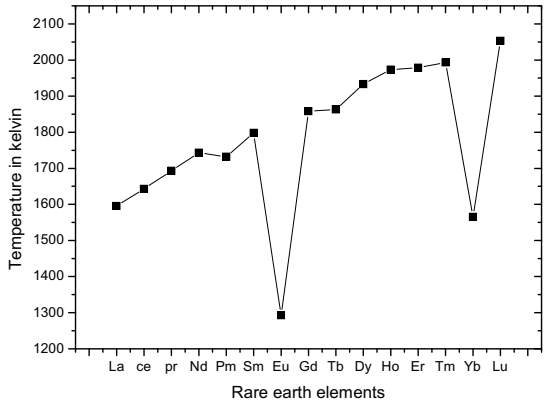

Fig. 1. Variation of the decomposition temperature of the equiatomic AuRE phase.

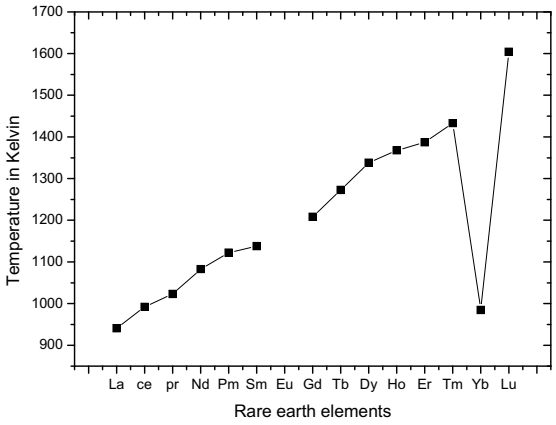

Fig. 2. Variation of the decomposition temperature of the $AuRE_2$ phase.

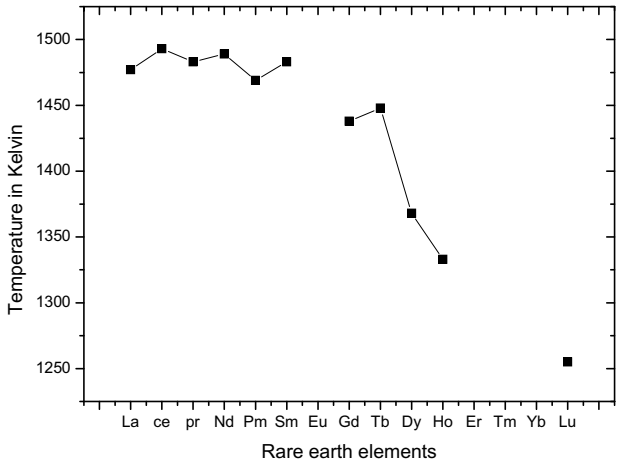

Fig. 3. Variation of the decomposition temperature of the $Au_{51}RE_{14}$ phase.

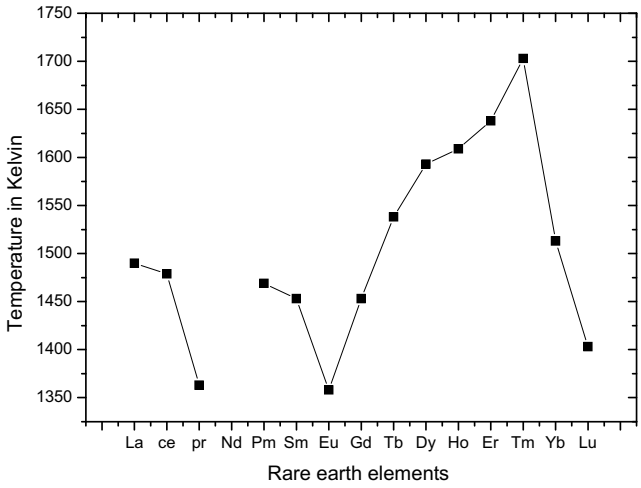

Fig. 4. Variation of the decomposition temperature of the Au_2RE phase.

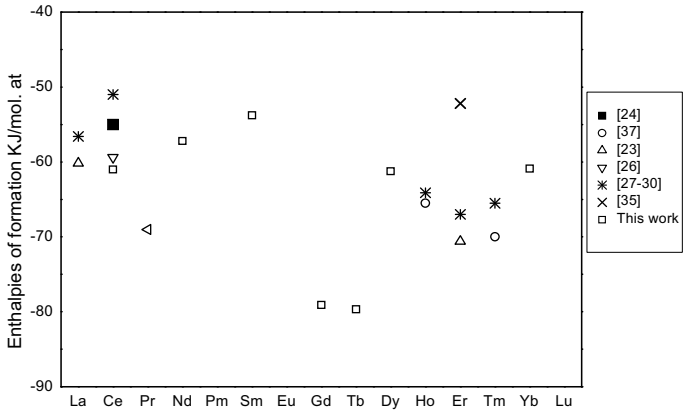

Fig. 5. Enthalpies of formation of the $AuRE_2$ phases.

3.3 Stoichiometric compounds

The Gibbs energy of the RE_pAu_q stoichiometric compound is expressed as follows:

$$ {}^0G_{RE_pAu_q} = \frac{p}{p+q}{}^0G_{RE} + \frac{q}{p+q}{}^0G_{Au} + a + bT \tag{6} $$

where ${}^0G_{RE}$ and ${}^0G_{Au}$are the Gibbs energy of the pure RE element and Au respectively. The "a" and "b" parameters are evaluated in the present work based on the literature data.

4 Results and discussion

4.1 Temperature of invariant reactions

The calculated Au-RE phase diagrams are in good agreement with the experimental results [1–4]. We compare here the Au-RE thermodynamic properties in order to gain

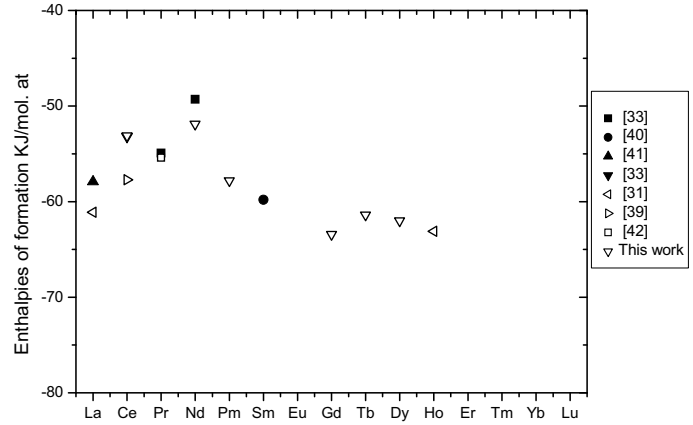

Fig. 6. Enthalpies of formation of the $Au_{51}RE_{14}$ phases.

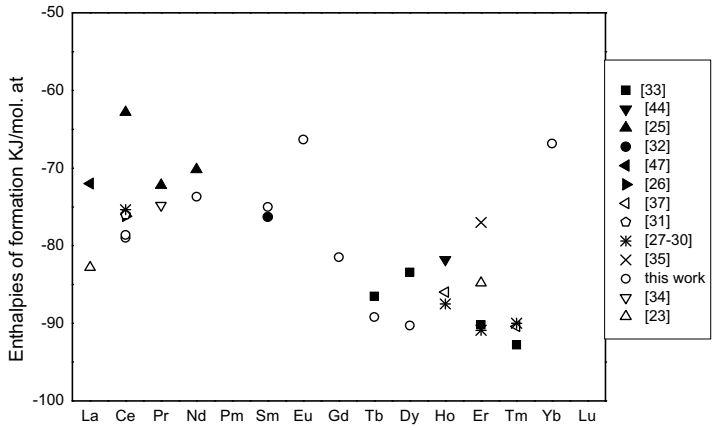

Fig. 7. Enthalpies of formation of the equiatomic AuRE phases.

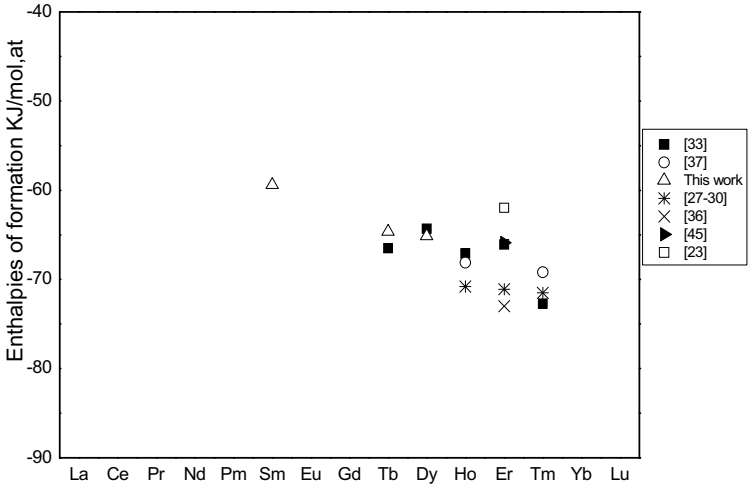

Fig. 8. Enthalpies of formation of the Au_3RE phases.

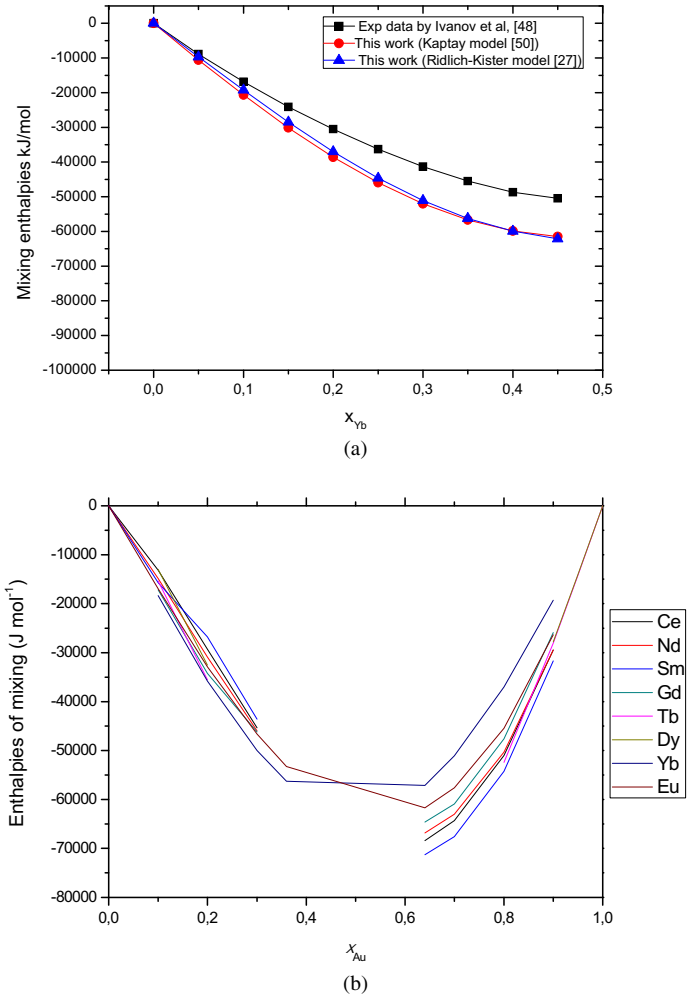

Fig. 9. (a) Mixing enthalpies of the Au-Yb liquid phase calculated at 1630 K by means of the Redlich-Kister and Kaptay models together with the experimental data by Ivanov et al. [48]. (b) Mixing enthalpies of the Au-RE liquid phase at 1630 K.

an overview and the trend of these parameters depending on the location of the rare earth element in their series. In this sense, we plot in Figures 1–4 the variation of the melting temperatures of the Au-RE phases which melt congruently. We note that this temperature increases linearly for the AuRE, $AuRE_2$ and Au_2RE phases and decreases for the $Au_{51}RE_{14}$ phases. Concerning the Au_2RE phases, this temperature appears to decrease for the light rare earth elements and increase for the heavy rare earths with an exception for the last two elements (Yb and Lu). These figures raise the already mentioned exception concerning the behavior of the Yb and Eu elements.

4.2 Enthalpies of formation

In Figures 5–8 we represent the enthalpies of formation of the Au-RE intermetallic compounds, calculated in this work using the PARROT module of the Thermo-Calc software [20] based on selected experimental and calculated data from the literature

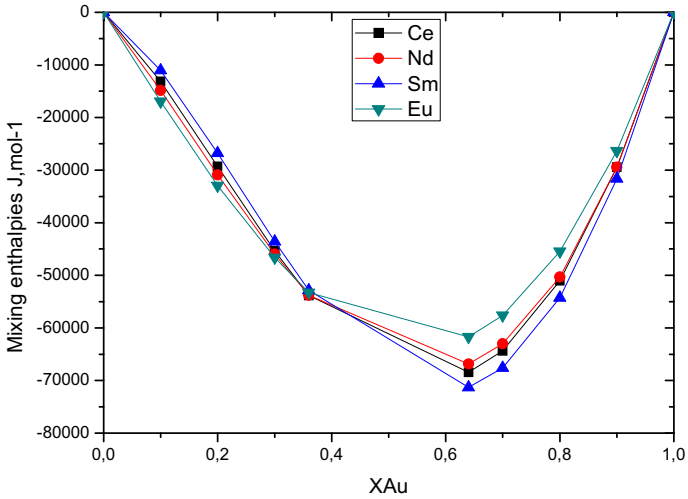

Fig. 10. Mixing enthalpies of the light Au-RE liquid phases calculated at 2000 K.

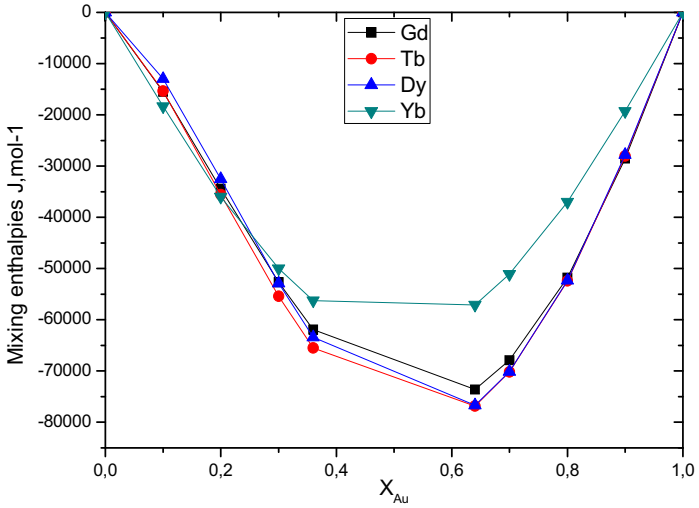

Fig. 11. Mixing enthalpies of the heavy Au-RE liquid phases calculated at 2000 K.

for the Au-RE systems (RE = Ce, Nd, Sm, Eu, Gd, Tb, Dy and Yb). According to the atomic number of the rare earth element, the experimental data are represented by filled shapes while values obtained from thermodynamic modeling and theoretical models are represented by symbols and empty asterisks respectively. The enthalpy of formation appears to increase significantly at the beginning of the series, tumble down in the middle of the series and finally remains almost constant for the heavy rare earths.

4.3 Mixing enthalpies of the liquid phases

Figure 9a shows the calculated mixing enthalpies of the Au-Yb liquid phase compared with the measured values at 1630 K by Ivanov et al. [48]. In Figure 9b we plot the values of the mixing enthalpies of the Au-RE liquid phases calculated at the same

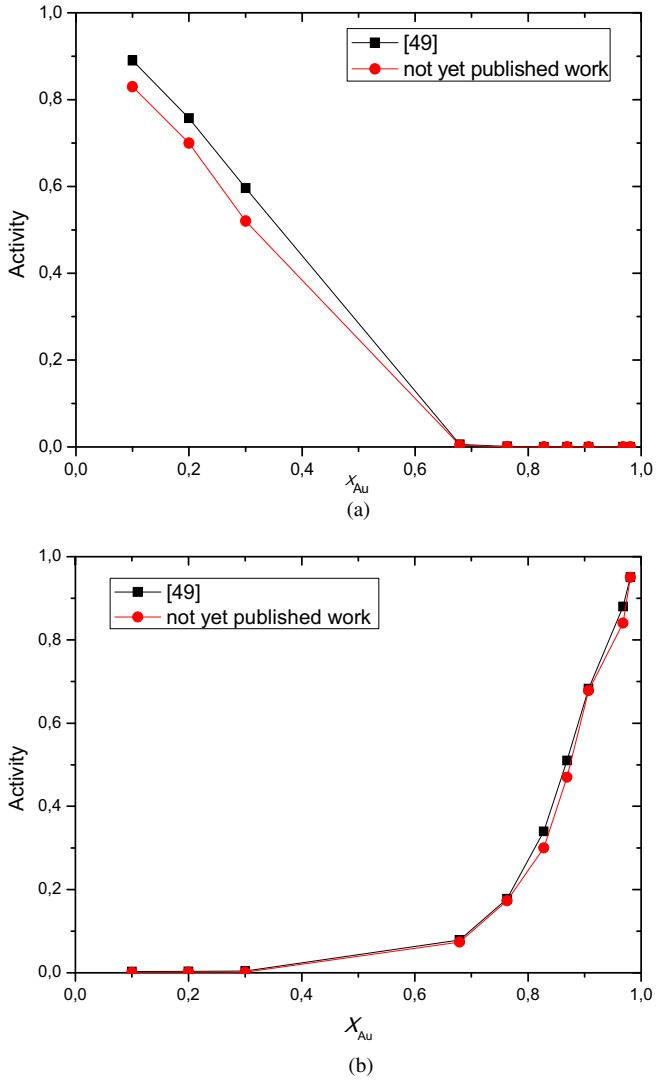

Fig. 12. (a) Variation of the activity of Gd in the Au-Gd system. (b) Variation of the activity of Au in the Au-Gd system.

temperature (1630 K). On the other hand we give in Figures 10–11, the enthalpies of mixing of the Au-RE liquid phases calculated at 2000 K. The most exothermic values of these enthalpies correspond rather to the elements located in the middle of the series. We note, once again, the particular behavior adopted by the Eu and Yb elements.

4.4 Activities

The only experimental activities of the Au-RE phases are those measured by Ivanov et al. [49] for the Au-Gd system. We compare in the Figures 12a and 12b, our calculated values with the experimental data available in the literature. In

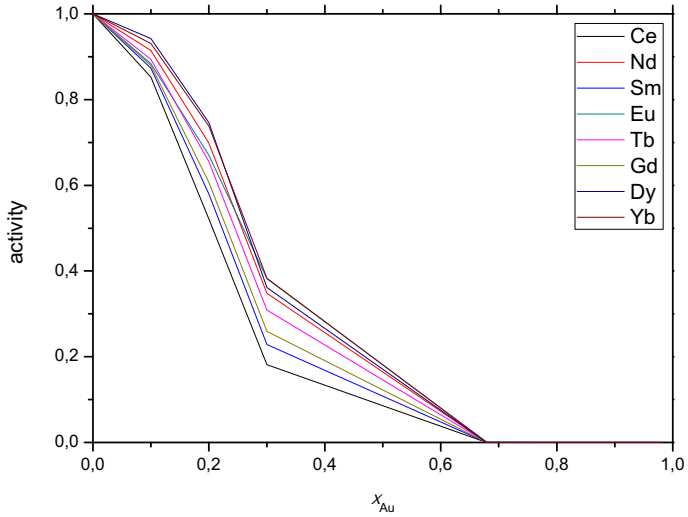

Fig. 13. Variation of the activity of RE in the Au-RE systems.

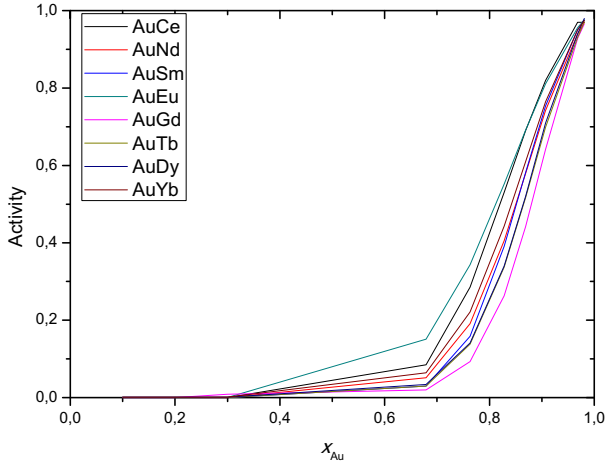

Fig. 14. Variation of the activity of Au in the Au-RE systems.

Figures 13 and 14 we give, for the first time, all the activities relative to the calculated Au-RE phase diagrams.

We note in this comparative study the exception of the Au-Yb and Au-Eu properties compared with those of the other Au-RE systems in the same series [1–4]. This particularity due basically to the fact that the electronic structure of the lanthanides elements (except Eu and Yb) can be schematically represented by a set of trivalent ions (Ln^{3+}) with the ($4f^n$) configuration and with three delocalized conduction electrons in a formed band from the 5d and 6s orbital while both Eu and Yb elements are described by a set of divalent ions (Ln^{2+}) (more voluminous than the ions (Ln^{3+})) with the ($4f^{n+1}$) configuration. Moreover the experimental studies of Eu-Au and Yb-Au alloy systems done by Johansson et al. [51] demonstrate that the chemical shifts of the surface core-level energies are different from the chemical shifts of the bulk core-level energies; they also showed that Eu and Yb segregates to the surface.

This could explain the singular behavior of the Au-Eu and Au-Yb systems compared with other Au-RE systems.

5 Conclusion

Au-Rare Earth (RE) (RE = Ce, Nd, Sm, Eu, Gd, Tb, Dy and Yb) binary systems have been systematically assessed and optimized based on the experimental and calculated data available in the literature. Particular emphasis was accorded to the observation of the trends and evolutions of the thermodynamic properties of the Au-RE phases. This work gives, for the first time, the thermodynamic quantities inaccessible to the experimental measurements and compare their variation versus the RE position. The Au-Eu and Au-Yb systems were found to behave differently in the studied Au-RE series, owing to the particular electronic structure of the Eu and Yb elements.

References

1. D. Moustaine, K. Mahdouk, J. Alloys Comp. **683**, 599 (2016)
2. D. Moustaine, K. Mahdouk, J. Alloys Comp. **673**, 115 (2016)
3. S. Otmani, K. Mahdouk, J. Alloys Comp. **670**, 369 (2016)
4. S. Otmani, K. Mahdouk, J. Alloys Comp. **648**, 581 (2015)
5. F.M. Seon, J. Less-common Met. **148**, 73 (1989)
6. H. Mavoori, A.G. Ramirez, S. Jin, J. Electron. Mater. **31**, 1160 (2002)
7. A.G. Ramirez, H. Mavoori, S. Jin, Appl. Phys. Lett. **80**, 398 (2002)
8. S. Jin, J. Electron. Mater. **32**, 1366 (2003)
9. C.A. Grimes, S.C. Roy, S. Rani, Q. Cai, Sensors **11**, 2809 (2011)
10. L. Kaufman, CALPHAD **1**, 7 (1977)
11. T.B. Massalski, H. Okamoto, P.R. Subramanian, L. Kacprzak (eds.), *Binary Alloy Phase Diagrams*, 2nd edn. (ASM International, Materials Park, OH, 1990)
12. M. Lomello-Tafin, A.A. Chaou, C. Antion, J.M. Moreau, J.C. Gachon, G. Coelho, in *Matériaux 2006, 13–17 November 2006, Dijon, France*
13. A. Saccone, D. Macciò, M. Giovannini, S. Delfino, J. Alloys Comp. **247**, 134 (1997)
14. A. Saccone, D. Maccio, S. Delfino, R. Ferro, Metall. Mater. Trans. A **30**, 1169 (1999)
15. A. Saccone, S. Delfino, R. Ferro, CALPHAD **14**, 151 (1990)
16. O.D. McMasters, K.A. Gschneidner, J. Less-Common Met. **30**, 325 (1973)
17. A. Palenzona, J. Less-Common Met. **100**, 135 (1984)
18. A. Saccone, M.L. Fornasini, D. Maccio, S. Delfino, Intermetallics **4**, 111 (1996)
19. A. Saccone, D. Maccio, S. Delfino, R. Ferro, Intermetallics **8**, 229 (2000)
20. A. Saccone, D. Maccio, S. Delfino, R. Ferro, Intermetallics **10**, 903 (2002)
21. A. Iandelli, A. Palenzona, J. Less-Common Met. **18**, 221 (1969)
22. Y. Ning, Gold bulletin **34**, 77 (2001)
23. O.D. McMasters, K.A. Gschneidner, G. Bruzzone, A. Palenzona, J. Less-Common Met. **25**, 135 (1971)
24. P.E. Rider, K.A. Gschneidner, O.D McMasters. Trans. Metall. **233**, 1488 (1965)
25. B. Jansson, Ph.D. thesis, Royal Institute of Technology, Staockolm, 1983
26. O. Anderesson, T. Helander, L. Höglund, P. Shi, B. Sundman, CALPHAD **26**, 273 (2002)
27. O. Redlich, A.T. Kister, Ind. Eng. Chem. **40**, 345 (1948)
28. A.T. Dinsdale, CALPHAD **15**, 317 (1991)
29. C.H. Lupis, *Chemical Thermodynamics of Metals* (Prentice-Hall Inc, North Holland, NY, 1983)
30. K.H. Kumar, P. Wollants, J. Alloys Comp. **320**, 189 (2001)
31. H.Q. Dong, X.M. Tao, H.S. Liu, T. Laurila, M. Paulastro-Kröckel. J. Alloys Comp. **509**, 4439 (2011)

32. R. Ferro, G. Borzone, N. Parodi, J. Alloys Comp. **321**, 248 (2001)
33. K. Fitzner, O.J. Kleppa, Metall. Trans. A **24**, 1827 (1993)
34. A. Janghorban, M. Lomello-Tafin, T. Mazingue, J. Chem. Thermodyn. **51**, 65 (2012)
35. P.E. Blöchel. Phys. Rev. B **50**, 17953 (1994)
36. G. Kresse, D. Joubert, Phys. Rev. B **59**, 1758 (1999)
37. J.P. Perdew, K. Burke, M. Ernzerhof, Phys. Rev. Lett. **77**, 3856 (1996)
38. H.J. Monkhorst, J.D. Pack, Phys. Rev. B **13**, 5188 (1976)
39. H.Q. Dong, X.M. Tao, T. Laurila, V. Vuorinen, M. Paulasto–Kröckel, CALPHAD **42**, 38 (2013)
40. S.V. Meschel, O.J. Kleppa, J. Alloys Comp. **416**, 93 (2006)
41. S.V. Meschel, O.J. Kleppa, J. Alloys Comp. **363**, 242 (2004)
42. Z. Du, C. Guo, D. Lü, J. Alloys Comp. **364**, 117 (2004)
43. Y. Wu, W. Hu, S. Han, J. Alloys Comp. **420**, 83 (2006)
44. K. Fitzner, O.J. Kleppa, Metall. Mat. Trans. **28**, 187 (1997)
45. H.Q. Dong, X.M. Tao, T. Laurila, M. Paulasto-Kröckel, CALPHAD **37**, 87 (2012)
46. R.A. Alqasmi, H.J. Schaller, J. Alloys Comp. **305**, 83 (2006)
47. R. Ferro, G. Borzone, N. Parodi, J. Alloys Comp. **321**, 248 (2001)
48. M.I. Ivanov, V.V. Berezutski, N.I. Usenko, J. Alloys Comp. **365**, L1 (2004)
49. M.I. Ivanov, V.V. Berezutski, J. Alloys Comp. **234**, 119 (1996)
50. G. Kaptay, Comput. Coupling Phase Diagrams Thermochem. **28**, 115 (2004)
51. L.I. Johansson, A. Flodstrom, S.E. Hornstrom, Surface Sci. **117**, 475 (1982)